SAND2022-13990

SANDIA REPORT

SAND20XX-XXXX
Printed September 2022

Sandia National Laboratories

The Strange Case of Ground-Coupled Airwaves on Seismoacoustic Stations at Local to Near-Regional Scales

Elizabeth M. Berg, Fransiska Dannemann Dugick, Sarah Albert, and Clinton Koch

Prepared by
Sandia National Laboratories
Albuquerque, New Mexico
87185 and Livermore,
California 94550

Issued by Sandia National Laboratories, operated for the United States Department of Energy by National Technology & Engineering Solutions of Sandia, LLC.

Available to DOE and DOE contractors from
U.S. Department of Energy
Office of Scientific and Technical Information
P.O. Box 62
Oak Ridge, TN 37831

Telephone: (865) 576-8401
Facsimile: (865) 576-5728
E-Mail: reports@osti.gov
Online ordering: http://www.osti.gov/scitech

Available to the public from
U.S. Department of Commerce
National Technical Information Service
5301 Shawnee Rd
Alexandria, VA 22312

Telephone: (800) 553-6847
Facsimile: (703) 605-6900
E-Mail: orders@ntis.gov
Online order: https://classic.ntis.gov/help/order-methods/

ABSTRACT

Here we investigate the application of ground-coupled airwaves observed by seismoacoustic stations at local to near-regional scales to detect signals of interest and determine back-azimuth information. Ground-coupled airwaves are created from incident pressure waves traveling through the atmosphere that couple to the earth and transmit as a seismic wave with retrograde elliptical motion. Previous studies at sub-local scales (<10 km from a source of interest) found the back-azimuth to the source could be accurately determined from seismoacoustic signals recorded by acoustic and 3-component seismic sensors spatially separated on the order of 10 to 150 m. The potential back-azimuth directions are estimated from the coherent signals between the acoustic and vertical seismic data, via a propagation-induced phase shift of the seismoacoustic signal. A unique solution is then informed by the particle motion of the 3-component seismic station, which was previously found to be less accurate than the seismoacoustic-sensor method. We investigate the applicability of this technique to greater source-receiver distances, from 50-100 km and up to 400 km, which contains pressure waves with tropospheric and stratospheric ray paths, respectively. Specifically, we analyze seismoacoustic sources with ground truth from rocket motor fuel elimination events at the Utah Test and Training Range (UTTR) as well as a 2020 rocket launch in Southern California. From these sources we observe evidence that while coherent signals can be seen from both sources on multiple seismoacoustic station pairs, the determined ground-coupled airwave back-azimuths are more complicated than results at more local scales. Our findings suggest more complex factors including incidence angle, coupling location, subsurface material, and atmospheric propagation effects need to be fully investigated before the ground-coupled airwave back-azimuth determination method can be applied or assessed at these further distances.

ACKNOWLEDGEMENTS

We acknowledge the efforts of Chip Brogan in generating the initial picks for the events analyzed in this report. We also greatly appreciate and acknowledge Marlon Ramos for his time and effort in providing a thorough technical review of this work. Furthermore, we appreciate and acknowledge Kathleen McKee for her insight, time, and energy in assisting us in using and testing her method.

This research was funded by the National Nuclear Security Administration, Defense Nuclear Nonproliferation Research and Development (NNSA DNN R&D). The authors acknowledge important interdisciplinary collaboration with scientists and engineers from LANL, LLNL, MSTS, PNNL, and SNL. This report describes objective technical results and analysis. Any subjective views or opinions that might be expressed in the paper do not necessarily represent the views of the U.S. Department of Energy or the United States Government. Sandia National Laboratories is a multimission laboratory managed and operated by National Technology & Engineering Solutions of Sandia, LLC, a wholly owned subsidiary of Honeywell International Inc., for the U.S. Department of Energy's National Nuclear Security Administration under contract DE-NA0003525.

CONTENTS

LIST OF FIGURES

This page left blank

ACRONYMS AND TERMS

Acronym/Term	Definition
GCA	Ground-Coupled Airwaves
GCA-BAD	Ground-Coupled Airwaves Back-Azimuth Determination
UTTR	Utah Test and Training Range

1. INTRODUCTION

Recent research from McKee et al. (2018) showed the ability for signal detection and back-azimuth determination of ground-coupled airwaves (GCA) on nearly collocated acoustic and seismic sensors. GCA are created from an incident pressure wave traveling through the atmosphere that grazes the Earth's surface (Ben-Menahem & Singh, 2000), coupling to the earth and transmitting as a seismic wave with retrograde elliptical motion (Ichihara et al., 2012). Initial results indicate that leveraging signals recorded by an infrasound sensor and three-component seismic sensor resulted in more accurate event back-azimuth, or direction of the source from the station, estimates than those from the seismic sensor's particle motion alone (McKee et al., 2018). This suggests the possibility that a seismoacoustic station, consisting of two nearly co-located sensors, separated by 10-100 m, could retrieve higher quality information than either a single infrasound or seismic sensor alone. We note that an infrasound array is also capable of obtaining back-azimuth information of airwave signals (e.g., Fuchs et al., 2019; Gibbons et al., 2015; Groot-Hedlin & Hedlin, 2014; Park et al., 2018). However, prior analysis of GCA showcased how a similar result can be achieved through a single collocated seismic and infrasound sensor (McKee et al., 2018). Therefore, this method may be more cost-effective, applicable to signals of variable distances from the source, and enable more creative deployments by increasing the potential distribution of sensors.

Previous research found that when an infrasound sensor is collocated with a vertical seismic sensor, there is a 90º phase shift between the respective recorded signals (Fee & Matoza, 2013; McKee et al., 2018). By increasing the distance between the seismic and infrasound sensors, seismoacoustic signals can be distinguished from correlated wind noise (Ichihara et al., 2012). McKee et al. (2018) found this spacing to be a maximum of 100 m, with an ideal spacing of 50 m. By combining the expected 90º phase shift and the known distance between seismic and acoustic sensors, the back-azimuth of the source can be estimated (McKee et al., 2018).

The Ground-Coupled Airwave-Back-Azimuth Detection method (GCA-BAD) first described by McKee et al. (2018) focused on waves at local distances of <15 km. At these distances, the incidence angle of the acoustic wave is near 90º from vertical along, or parallel to, the surface (McKee et al., 2018; Fee & Matoza, 2013). However, McKee et al. (2018) also discussed the potential to use the GCA-BAD method with acoustic arrivals from waves traveling through further layers of the atmosphere, including the troposphere, which have incidence angles around 90º, stratosphere, with incidence angles of <79º, and thermosphere, which have incidence angles of ~60º (McKee et al., 2018; Fee et al., 2013). Our work here tests the GCA-BAD method at further distances using tropospheric and stratospheric arrivals.

2. GROUND-COUPLED AIRWAVE (GCA) BACK-AZIMUTH DETERMINATION (BAD) METHOD

The GCA-BAD method is covered in detail within McKee et al. (2018), but we review the main steps here with the aid of a diagram (Figure 1) adapted from McKee et al. (2018) for clarity. This method is applicable to far-field observations from a source, or distances in which pressure and particle velocity are in-phase with one another (Smith & Gabrielson, 2020). Additionally, this method is only suitable to seismoacoustic stations consisting of a seismic sensor (orange) at distance *d*, ranging from 10 to 100 m, from the infrasound sensor (green), as shown in Figure 1a. Unlike the distance between stations, any orientation of the sensors is appropriate for this method, shown in the example as azimuth between the stations, β (see Figure 1a). To obtain the back-azimuth, the direction of the event from the seismic sensor, we first determine the coherency between the vertical seismic data and infrasound omnidirectional data (Figure 1b) to assess existence of GCA. Coherency is estimated for frequencies with 1Hz steps, from 0 to the Nyquist frequency, and over a given time with 90% overlapping windows. The coherence for each frequency and time window is calculated, and those with values > 0.75 are retained.

Following the coherency assessment, the infrasound data is shifted in time to maximize the expected 90º phase shift between the vertical seismic and infrasound sensor (McKee et al., 2018; Fee & Matoza 2013). First, the minimum and maximum time shift is determined, as $-d/c$ to d/c, where c is the acoustic wave speed, set to 330 m/s for the stratospheric case and 343 m/s for the tropospheric cases below. We then shift the infrasound data between these times, with a time-step of dt/4, where dt is the sample rate time of 0.02 s for the data analyzed in this study. For each time shift, we calculate the corresponding phase spectrogram (see Figure 1c). Once we calculate the sum of the phases (visually represented in the phase spectrogram) at each time-shift, we make a histogram of the back-azimuth distribution (Figure 1d). This is determined from the time-shift and assumed wave speed as $d_0 = -c \Delta t$ and $\theta = cos^{-1}(d_0/d)$, with the resulting back-azimuth = $\beta \pm \theta$. We note that any optimal time-shift corresponds to two back-azimuths.

Finally, we determine the final back-azimuth from the two GCA-BAD results as that in agreement with the 3-component seismic sensor's retrograde elliptical motion. First, we determine the existence of retrograde elliptical particle motion on the seismic sensor, and then we use the Coherency Matrix method (Vidale, 1986) to assess the particle motion azimuth through time, corresponding to the direction of the source. We note that the retrograde elliptical particle motion will have energy minimized in the transverse direction, with a 90º phase shift between the vertical and radial directions, respectively (Figure 1e). While the seismic sensor's particle motion is sensitive to the source direction, it is also prone to a variety of known issues. The most major of these is sensitivity to heterogeneities in the local geology that can cause very large uncertainties (>40º) in back-azimuths derived from particle motions. As a result, back-azimuths from seismic particle motion are not reliable for determining an accurate direction of arrival, but they can be used to resolve the general direction of the source to inform the GCA-BAD method results.

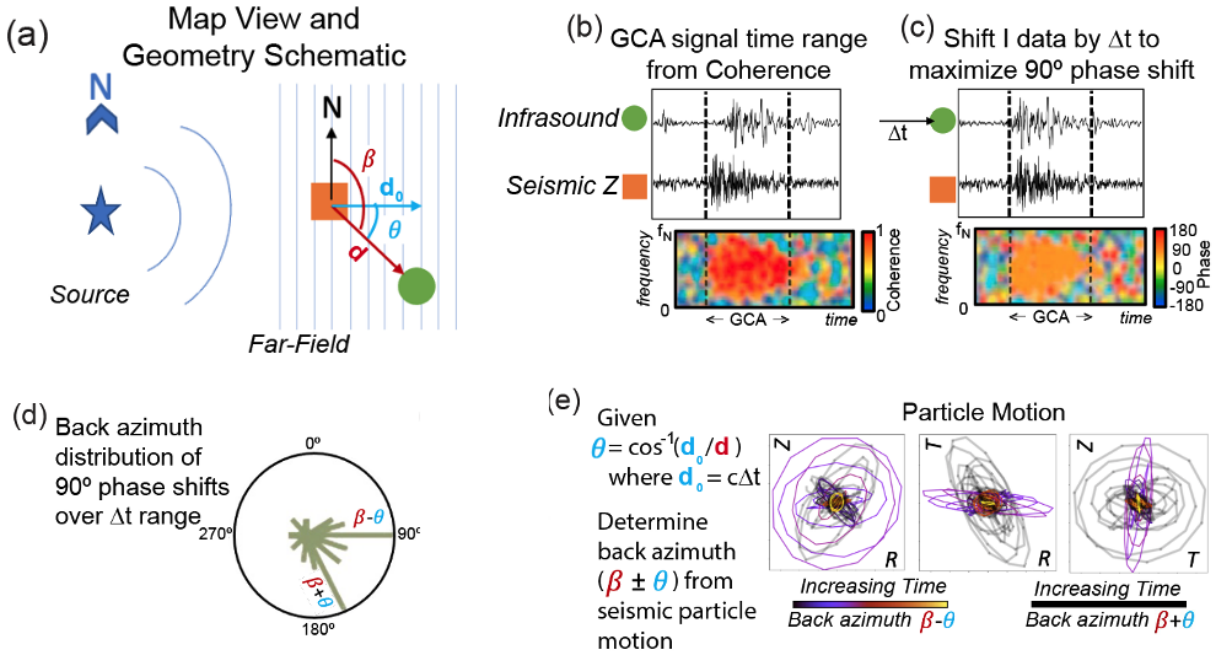

Figure 1. Overview of GCA Back-Azimuth Detection method using infrasound and 3-component seismic sensors. Adapted from McKee et al. (2018). Refer to section 2 for major data processing steps.

3. RESULTS & DISCUSSION

We consider two types of sources in our analysis of seismoacoustic data at local to near-regional scales. We first analyze rocket motor fuel elimination explosion events at the Utah Test and Training Range (UTTR), with seismoacoustic stations located at 44-74 km from the source. We determined via acoustic ray-tracing (Blom & Waxler, 2012; Blom, 2022) that the GCA signals at these stations consist of tropospheric arrivals. Importantly, Park et al. (2018) analyzed these seismic and acoustic datasets independent of one another, whereas in this work we evaluate the ability to use the signals together to assess source location. Second, we consider a rocket launch in Southern California recorded on stations 400 km from the event, with signals consisting of stratospheric arrivals.

3.1. UTTR Explosion – Tropospheric Arrivals

The UTTR rocket motor fuel elimination explosion events are recorded on a variety of seismic and infrasound sensors (see Figure 2). However, due to the limited number of available and recording infrasound sensors, we only have six possible sets of seismoacoustic station locations applicable to the GCA-BAD method. This alone highlights the difficulty of assessing this method, as the few seismoacoustic stations for this event are all within 100 km of the source. However, as shown in Figure 2, there are a significant number of seismic stations that record coupled infrasound signals, which suggests this method could be suitable for event analysis if infrasound sensors are added to existing seismic networks.

We first analyze GCA signals recorded by seismic station HVU and infrasound station HVU5, detailing the GCA-BAD processing of signals and results from the August 1, 2007, UTTR event. Following this demonstration of the GCA-BAD method to real data, we next consider results from multiple seismoacoustic station pairs for the same August 1, 2007, UTTR event. Finally, we analyze results from multiple UTTR events to assess consistency of the GCA-BAD method results.

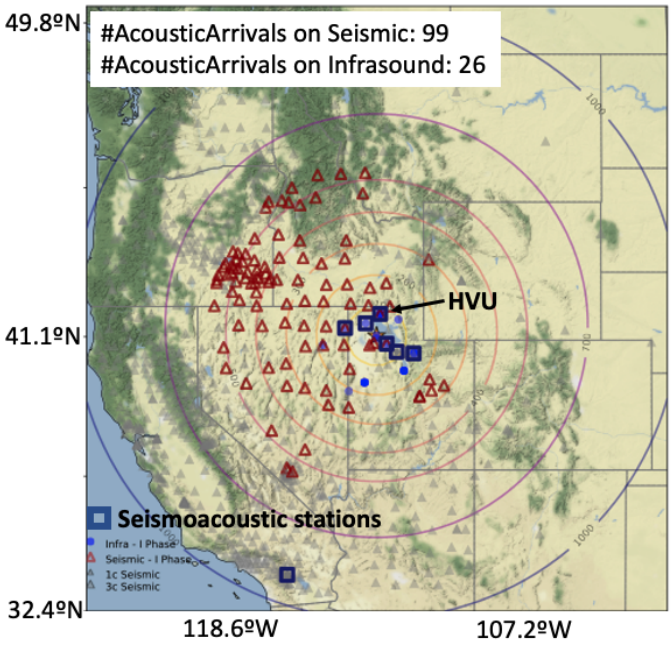

Figure 2. Map of seismic and infrasound stations recording at the time of the UTTR explosion on August 1, 2007. Blue circles denote infrasound stations with recorded acoustic signals, while red triangles denote seismic stations with recorded acoustic signals that coupled and transmitted into the subsurface. Blue squares denote locations of seismoacoustic sensors with signals potentially applicable to the GCA-BAD method. The increasing, labeled in kilometer units, circles denote increasing distance from the source.

3.1.1. Detailed Results from Single Seismoacoustic Station Pair

We first consider seismic station HVU, located 74 km north of the source, and infrasound station HVU5, located 77 m west from HVU. In Figure 3, we show the raw data recorded by both sensors in both the time and frequency domains. Expected signal arrival times, based on the known event source time derived from ak135 for seismic and typical propagation speeds for infrasound (Kulichkov, 2000; Nippress et al., 2014), are plotted as red (seismic) and pink (infrasound) vertical lines. On the raw seismic data (Fig 3 a and b), we observe multiple signals, including a significant amplitude increase following the expected P-wave arrival and surrounding the predicted tropospheric arrival time. We also note that the tropospheric, *Iw* (see Fig 3 b), arrival appears clearer within the seismic spectra across all considered frequencies. We do not see a stratospheric arrival, but there is some evidence of a late arrival that may be a thermospheric, *It* (see Fig 3 a-b), signal but may also be unrelated to this event. On the infrasound data (Fig 3 c-d) we observe a large signal around the tropospheric arrival predicted time, but we do not observe any other clear signals.

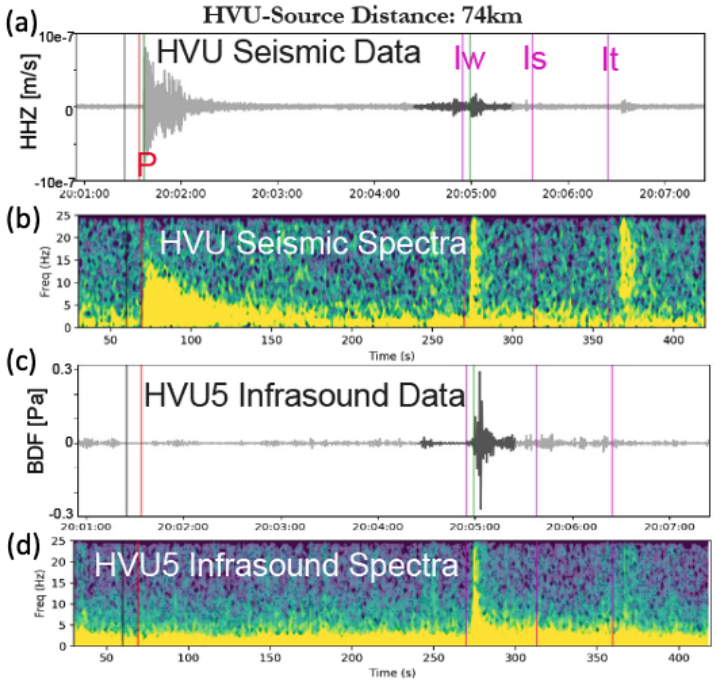

Figure 3. August 1, 2007 UTTR event signals recorded by seismic station HVU and infrasound station HVU5 including time-series (a) of seismic data on the vertical component, with ground-truth event origin time (black), predicted (red) and observed (green) P-wave, as well as predicted (pink) and seismic-analyst picked (green) infrasound arrivals. The spectra of the (b) seismic data are also denoted in this manner. Similarly labeled, the HVU5 infrasound (c) time-series and (d) spectra are shown. The data considered for analysis is denoted in black, while the full time-series for both are in gray.

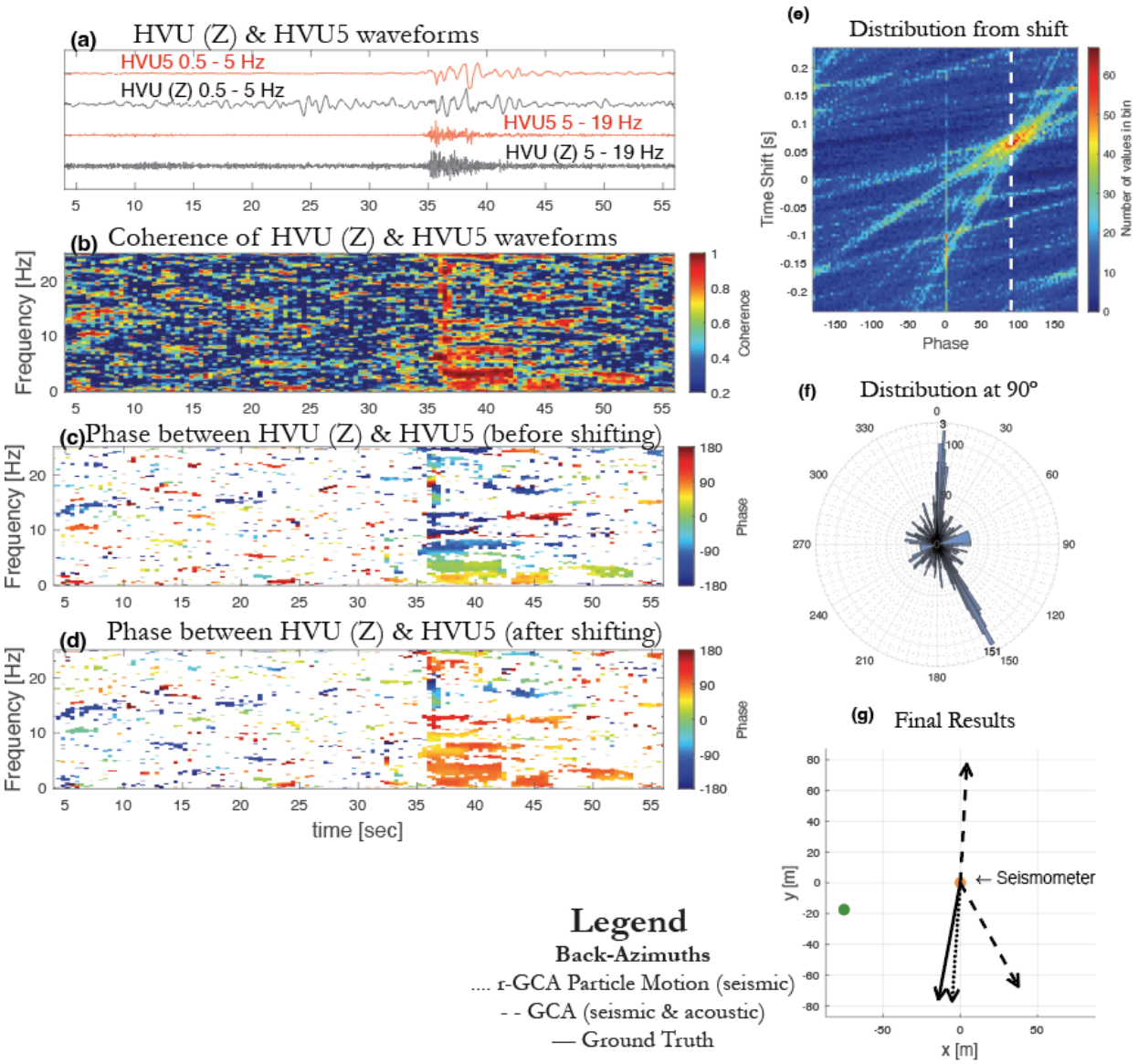

Figure 4. GCA-BAD method results applied to vertical component of seismic station HVU and infrasound station HVU5. (a) Filtered time-series of infrasound (red) and seismic (black) data. (b) Coherence between seismic and infrasound spectra. (c) Initial phase observed across the various frequencies for bins with coherence > 0.75, and, similarly, (d) after time-shifting to maximize 90º phase shift. (e) Distribution of the number of results in each time-shifted bin for each phase, with 90º denoted in a white dashed line. (f) Distribution at 90º and corresponding back-azimuth results. (g) Final results of directionality from the seismometer using data recorded by seismic (orange dot) and infrasound (green dot) sensors, including ground-truth (solid arrow), GCA-BAD method predictions (dashed), and seismic station particle motion (dotted).

We next consider the filtered data from the seismic and infrasound time-series (Figure 4a). We visually observe significant similarities between the two waveform packets around 35-40 seconds within the selected window of data. Additionally, these data sections contain high coherence (Figure 4b), which indicates the presence of the same signal propagating and being recorded across both sensors. We observe that the phase angles, prior to shifting the infrasound data, are highly variable

over 0.1-20 Hz (see Fig 4 c). However, following the time-shifting procedure, we observe 90º phase-shift within this section of data below approximately 10 Hz (see Fig 4 d). There is also a clear stack of signals at 90º with a time shift of 0.07 seconds (Figure 4e). With this information, we calculate the distribution of back-azimuths (Figure 4f); high-confidence results are found with back-azimuths of 4º and 150º (each with a total of 100 binned results). Nonetheless, we observe that these back-azimuths do not agree well with the ground-truth back-azimuth (Figure 4g). In contrast, the back-azimuth estimated from direction of retrograde elliptical motion from the seismic data alone better agrees with the ground-truth.

These results contradict the findings from more local-scale examples in McKee et al. (2018) and suggests higher complexity at this local to near-regional scale, as the method is clearly able to robustly resolve the time-shift necessary to obtain a phase angle of 90º between the seismic and infrasound data. In fact, a 180º shift is apparent between one of the predicted back-azimuth results and the known back-azimuth. This may be a result of the infrasound instrument response or coupling effects from the GCA. However, this is the result from analysis at a single station. In the following sections we consider more seismoacoustic station pairs and UTTR events to assess the underlying cause of observed errors.

3.1.2. Results from Multiple Seismoacoustic Stations for a Single Event

We next consider results from multiple nearly collocated seismoacoustic stations. These stations are at variable azimuths from the UTTR site (see Figure 5). However, only the labeled seismoacoustic stations have coherent signals between the seismic and infrasound sensors, as not all seismoacoustic sensor pairs (Figure 2 and Figure 5) had consistent, robust, or coherent signals for analysis. Specifically, only six stations recorded signals near arrival times predicted from ray-tracing, with great enough signal-to-noise ratios for GCA-BAD analysis, and were coherent across both seismic and infrasound sensors. On applicable seismoacoustic stations, we repeat the same analysis described above and find that seismoacoustic signals from these stations robustly resolve the time-shift necessary to obtain a phase angle of 90º between vertical seismic and infrasound signals, with majority of resolvable signal being less than 10 Hz.

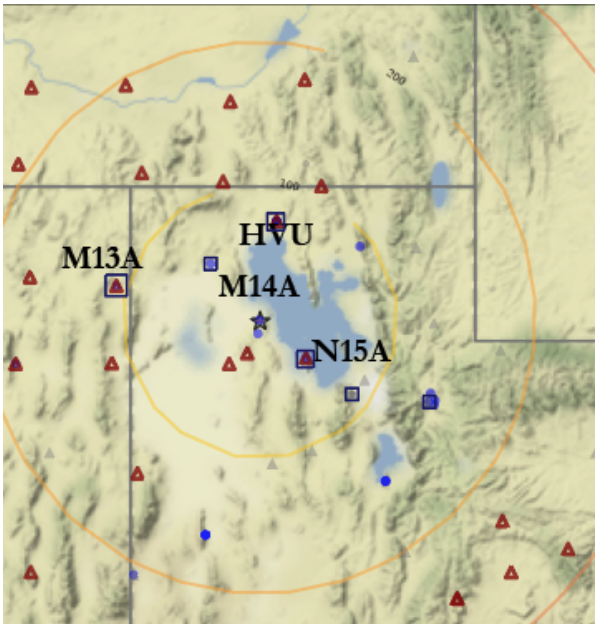

Figure 5. Zoomed in map of the distribution of seismoacoustic stations (see Figure 2), denoted with squares, compared to the event location (star). Large circles denote incremental distances of 100km from the source.

We show the results from all coherent signals, similar to Figure 4g, for all seismoacoustic station pairs labeled in Figure 6. We do not consistently observe the 180º discrepancy seen at station HVU, which suggests that an incorrect application of the instrument response correction is unlikely. Instead, it appears that the GCA-BAD method may need additional corrections (topography, atmospheric propagation effects, subsurface material impact, etc.) at distances further from a source of interest than considered in previous research. Alternatively, the GCA-BAD method may simply not be appropriate at these distances, as a wide spread of results is apparent for the various seismoacoustic stations.

Additionally, it appears that the seismic station's back-azimuth is consistent to the ground-truth for two of these stations, but not for N15A. This indicates that N15A may have topographic or coupling effects associated with the subsurface material that need to be considered. As shown in Figure A-1, this seismoacoustic pair also has a focused time-shift near 50º instead of 90º, which supports a more-complicated signal that may not be a ground-coupled airwave. In contrast, the seismoacoustic array consisting of M13A and M13A1 also does not resolve the ground truth with the GCA-BAD method but does show clustering of the time-shift around 90º (see Figure A-2).

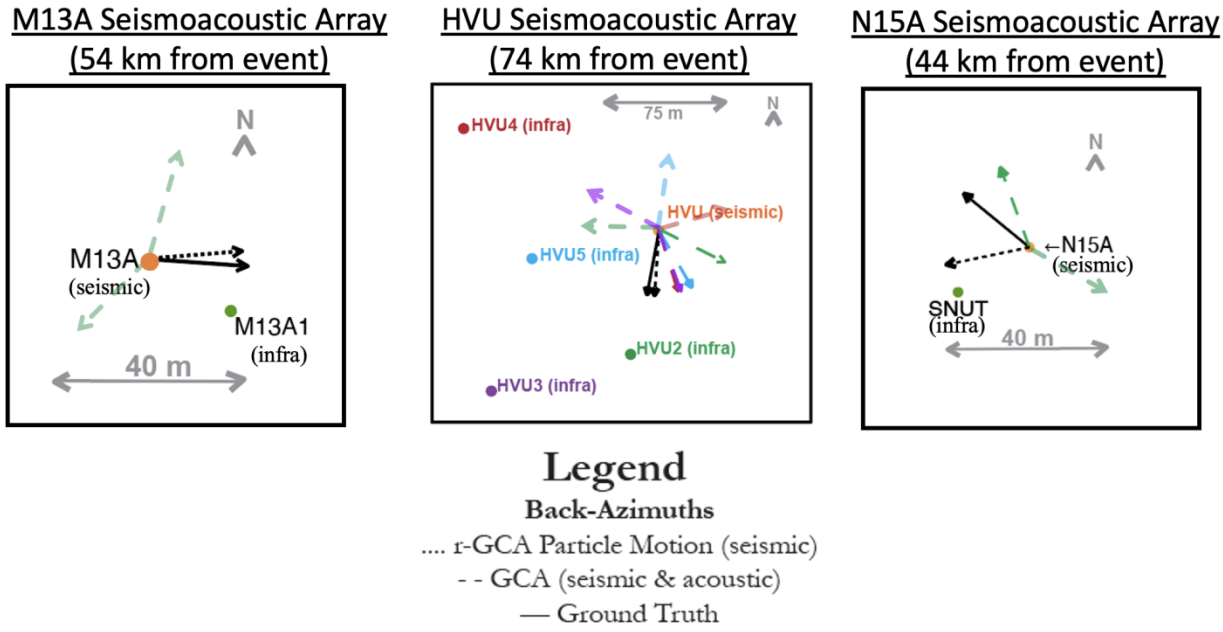

Figure 6. Back-azimuth results for the GCA-BAD method (dashed lines) and seismic particle motion (dotted lines) compared to ground-truth (solid line) for seismoacoustic station pairs with seismic stations M13A, HVU, and N15A. GCA-BAD results for are colored according to corresponding infrasound station (colored similarly). We observe the seismic retrograde elliptical (black dotted line) typically out-performs the GCA-BAD method (colored dashed lines) to match ground-truth (solid black line).

3.1.3. Results from Multiple Events

We also analyze multiple UTTR events recorded by the previously shown seismoacoustic stations in Figure 5 to further assess applicability of GCA. Notably, the HVU seismoacoustic stations record coherent GCA signals for events on August 1, 2007, and June 6, 2007, whereas the M13A and M14A stations record signals from the August 1, 2007, and August 27, 2007, events. However, the N15A station records signals from August 1, 2007, August 27, 2007, and June 6, 2007, events. This points to high variability and that stations closer to the event (< 50 km) are likely to capture GCA signals on both seismic and acoustic stations, which suggests seismoacoustic signals are less impacted by atmospheric conditions and transmission loss at distances closer to the event.

Notably, we do not see a consistency in the 180° signal variation. Instead, we observe high variability between ground truth and GCA-BAD results. Additionally, the particle motion estimated from the seismic station alone appears to be overall more consistently aligned with the ground truth compared to results from the GCA-BAD method. This supports the need for further corrections to address increased complexities with the GCA-BAD method at these scales.

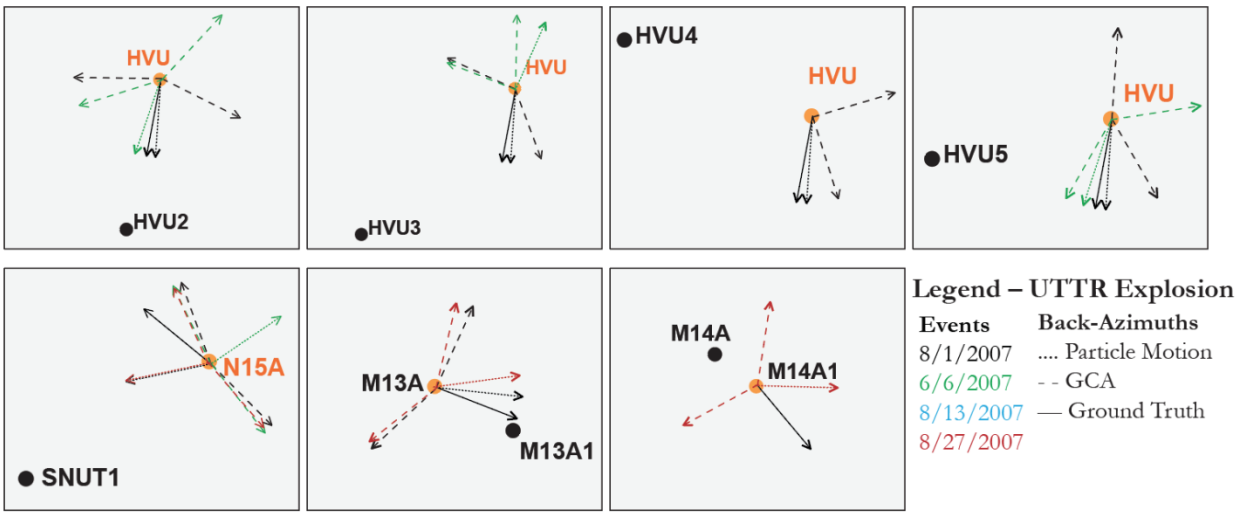

Figure 7. Results from multiple UTTR events at a variety of seismoacoustic stations.

3.2. California Rocket Launch – Stratospheric Arrivals

We next analyze signals from a rocket launch in Southern California at stations 400 km from the event. Acoustic ray-tracing analysis predicts stratospheric arrivals would be observed at these distances from the source. We consider two sets of seismoacoustic stations but show the results for the BPH11 seismic station in the main report, with the more convoluted results associated with BPH03 included in the Appendix (Figure A-3). In Figure 8, we show a map of the origin location and seismic and infrasound stations that record acoustic signals, as picked by a seismic analyst. Notably, although the region has a dense network of seismic stations, only a seemingly random subset detects acoustic signals, without an obvious preferred distance or direction. This may be an effect of topography or atmosphere, but this phenomenon is an area of research for future work. This region has very few infrasound sensors, but those in place are collocated with seismic stations such that the GCA-BAD method is applicable.

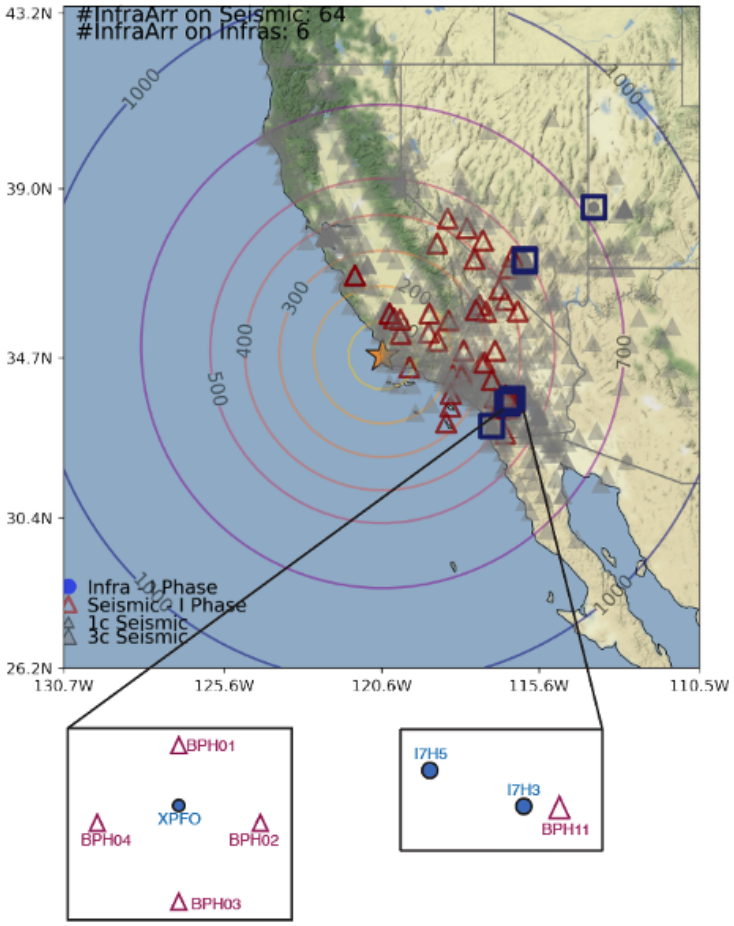

Figure 8. Station map of the November 21, 2020, rocket launch out of Southern California. Red triangles denote 3-component seismic stations with acoustic signals, blue circles denote infrasound stations with acoustic signals, and blue squares denote seismoacoustic stations with separation distances that make the signals applicable to the GCA-BAD method.

3.2.1. Detailed Results from Single Seismoacoustic Station Pair

We first analyze the time-series and spectra from the rocket launch recorded by the BHP11 seismic and I57H3 infrasound sensors. As shown in Figure 9, the seismic signal on BPH11 is rather weak in the time-domain, although clear peaks appear in the spectra above 10 Hz following the predicted P arrival time that may be signal related to the rocket launch event. However, the stratospheric arrival does contain stronger signal at frequencies < 10-15 Hz. Similarly, the infrasound sensor detects signal around less than 10-15 Hz. Both signal packets look complex in that there are three distinct packets of arrivals. As this is a rocket launch, we expect a more complex waveform and the signal to be poorly coupled to the Earth, so our observations, weak seismic signals and stronger but complex acoustic signals, are consistent to what we expect for this event.

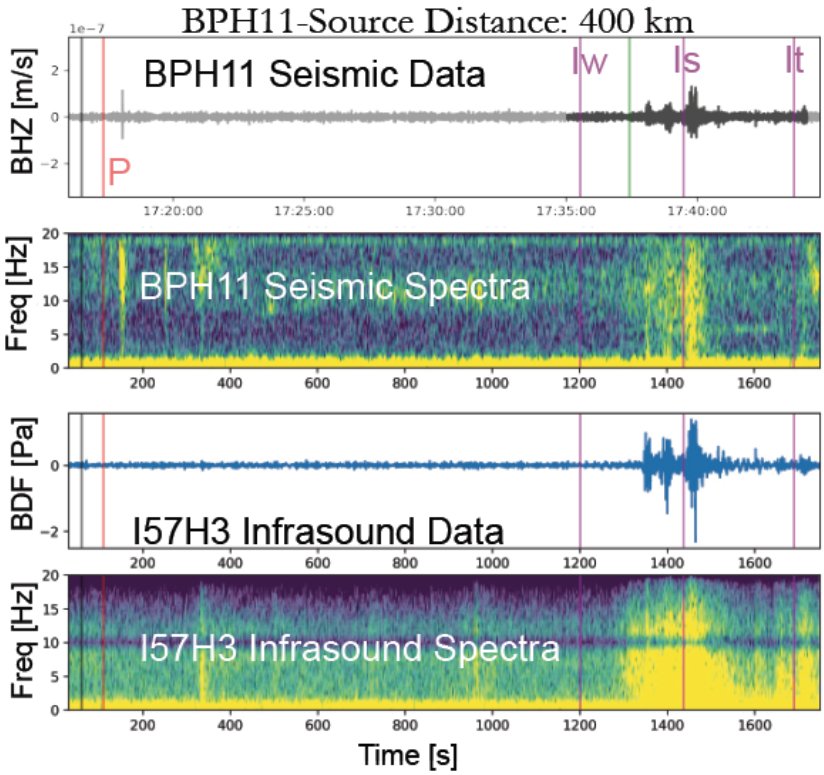

Figure 9. Similar to Figure 3, but for BPHll seismic and I7H3 infrasound stations recording signals from the Nov 21, 2020, rocket launch.

As shown in Figure 10, we apply the GCA-BAD method to this data and observe coherent signals between the seismic and infrasound data below 10 Hz across all three wave packets of energy. Interestingly, when we apply the time-shift (Figure 10c) we do see a grouping around 90º, although stratospheric arrivals have an incidence angle of <79º compared to a 90º incidence angle for tropospheric arrivals as considered previously. The effect of a non-90º incidence angle for GCA recorded by seismic stations is an area of future research. Using the 90º time-shift results, we end up with a broader distribution of back-azimuth estimates than the tropospheric results from the UTTR explosion, shown in Figure 10g. Additionally, the back-azimuth estimates are not in agreement with the ground-truth direction (Figure 10h). Furthermore, the particle motion from the seismic station is also not in agreement with the expected ground truth. This may be caused by topography, atmospheric effects, or attributed to the complex source.

In Figure 11 we show the results from BPH11 and I57H3 as well as from BPH11 and I57H5. The GCA-BAD results are consistent between the two pairs, but the particle motion is aligned with the GCA-BAD method for the latter and not the former. Both pairs showed a focused time-shift around 90º, which is not expected for stratospheric arrivals. The XPFO and BPH03 seismoacoustic pair also did not result in a 90º grouping, but instead contains a cluster around 145º (see Figure A-3). These results demonstrate the need to better understand the nature of GCA at these distances before adapting the GCA-BAD method.

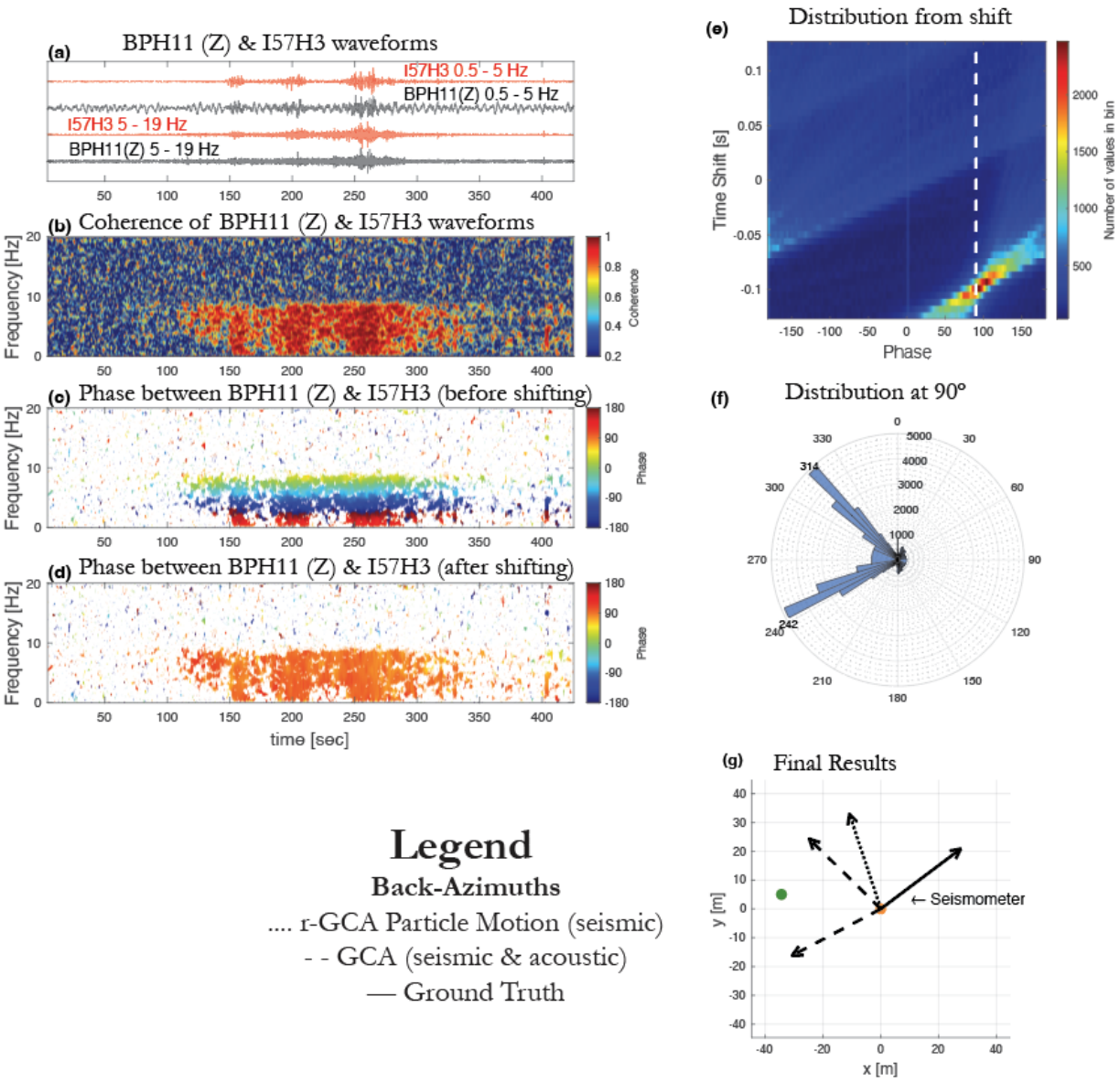

Figure 10. GCA-BAD method results of signals from the Nov 21, 2020, rocket launch recorded by seismic station BPH11 and infrasound station I57H3, both of which are 400 km from the source and with a station separation of 30 m.

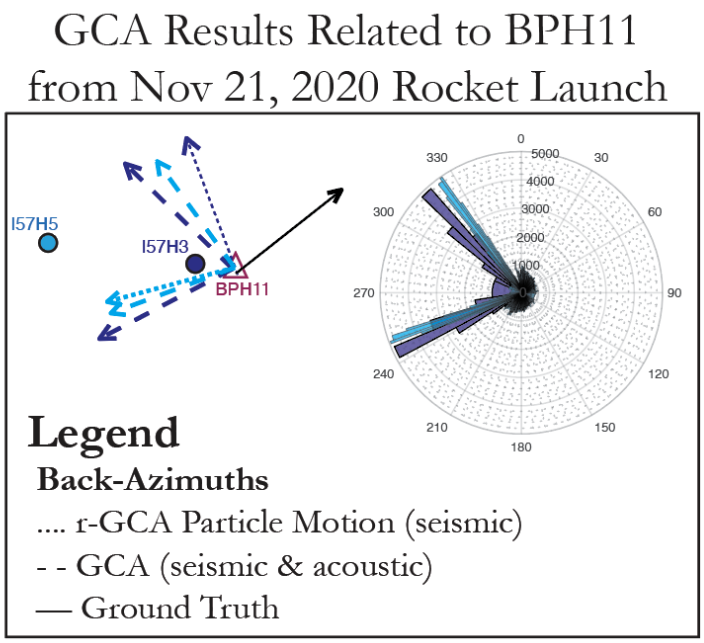

Figure 11. Summary of GCA-BAD back-azimuth estimates of the Nov 21, 2020, rocket launch using seismic station BPH11 and infrasound stations I57H5 (or I7H5) and I57H3 (or I7H3).

4. CONCLUSIONS & LOOKING FORWARD

In this report we evaluated the validity of the GCA-BAD method by analyzing recordings of infrasound arrivals from multiple sources of interest. We investigated tropospheric and stratospheric arrivals recorded at nearly collocated seismic and acoustic station pairs, at distances of 50-100 km and 400 km, respectively. By testing this method with ground-truth sources, we can compare back-azimuths estimated via the GCA-BAD method to those calculated from the known source and receiver locations. These comparisons indicate that the GCA-BAD method does not reliably produce back-estimates estimates comparable to the ground-truth.

However, we do find particle motion of GCA on seismic stations is overall retrograde elliptical (see Figure A-4), and that back-azimuth estimates from seismic particle motion tend to be more in line with the ground-truth. Additionally, we find that signals are coherent between seismic and infrasound stations at these local to near-regional scales, indicating that a method focused on evaluating coherency may be useful in identifying GCA arrivals. These type of seismoacoustic arrivals could then be used in event location analysis (e.g., Koch & Arrowsmith, 2019; Park et al., 2018). However, significant work is needed to assess how seismic stations record GCAs, as GCA arrivals may be affected by topography, subsurface material, atmospheric propagation path effects, and more. Recent research demonstrates that subsurface material greatly impacts ability to record GCAs at the sub-local-scale of 2-10 km from a source of interest (Anthony et al., 2022), but similar investigation of GCAs remains at local, local-to-regional, and regional scales. Luckily, as demonstrated within this report (see Figures 2, 5, and 8) many three-component seismic stations exist that have recorded GCAs.

As we highlighted in this study, there are very few historical seismic and infrasound station pairs with appropriate separation distance to be applicable to the GCA-BAD method. The coherency between seismic and acoustic stations does not require stations to have a certain separation but can be used on perfectly collocated or slightly separated stations, albeit local wind effects may dampen the coherency if not ideally separated or perfectly collocated. Thus, the coherency of GCAs by seismic and infrasound sensors may also be an avenue for future research into signal detection techniques.

REFERENCES

Anthony, R. E., Watzak, J., Ringler, A. T., & Wilson, D. C. (2022). Characteristics, relationships and precision of direct acoustic-to-seismic coupling measurements from local explosions. *Geophysical Journal International*, *230*(3), 2019–2035. https://doi.org/10.1093/gji/ggac154

Ben-Menahem, A., & Singh, S. J. (2000). Seismic waves and sources (2nd ed.). New York: Springer. https://doi.org/10.1007/978-1-4612-5856-8

Blom, P., & Waxler, R. (2012). Impulse propagation in the nocturnal boundary layer: Analysis of the geometric component. *The Journal of the Acoustical Society of America*, *131*(5), 3680-3690.

Blom, P. S. (2022). *stochprop Documentation, Release 1.0* (No. LA-UR-21-32412). Los Alamos National Lab.(LANL), Los Alamos, NM (United States).

Fee, D., McNutt, S. R., Lopez, T. M., Arnoult, K. M., Szuberla, C. A. L., & Olson, J. V. (2013). Combining local and remote infrasound recordings from the 2009 Redoubt Volcano eruption. Journal of Volcanology and Geothermal Research, 259(C), 100–114. https://doi.org/10.1016/j. jvolgeores.2011.09.012

Fee, D., & Matoza, R. S. (2013). An overview of volcano infrasound: From hawaiian to plinian, local to global. Journal of Volcanology and Geothermal Research, 249, 123–139. https://doi.org/10.1016/j.jvolgeores.2012.09.002

Fuchs, F., Schneider, F. M., Kolínský, P., Serafin, S., & Bokelmann, G. (2019). Rich observations of local and regional infrasound phases made by the AlpArray seismic network after refinery explosion. *Scientific Reports*, *9*, 13027. https://doi.org/10.1038/s41598-019-49494-2

Gibbons, S. J., Kværna, T., & Mykkeltveit, S. (2015). Could the IMS Infrasound Stations Support a Global Network of Small Aperture Seismic Arrays? *Seismological Research Letters*, *86*(4), 1148–1159. https://doi.org/10.1785/0220150068

Groot-Hedlin, C. D., & Hedlin, M. A. (2014). Infrasound detection of the Chelyabinsk meteor at the USArray. *Earth and Planetary Science Letters*, *402*, 337–345. https://doi.org/10.1016/j.epsl.2014.01.031

Ichihara, M., Takeo, M., Yokoo, A., Oikawa, J., & Ohminato, T. (2012). Monitoring volcanic activity using correlation patterns between infrasound and ground motion. Geophysical Research Letters, 39, L04304. https://doi.org/10.1029/2011GL050542

Koch, C. D., & Arrowsmith, S. J. (2019). Locating surface explosions by combining seismic and infrasound data. *Seismological Research Letters*, *90*(4), 1619–1626. https://doi.org/10.1785/0220190017

Kulichkov S.N. On infrasonic arrivals in the zone of geometric shadow at long distances from surface explosions, *Proceedings of the Ninth Annual Symposium on Long-Range Propagation*, 2000. Oxford, Mississippi, 14–15 September, National Center for Physical Acoustics (pg. 238-251).

McKee, K., Fee, D., Haney, M., Matoza, R., & Lyons, J. (2018). Infrasound Signal Detection and Back Azimuth Estimation Using Ground-Coupled Airwaves on a Seismo-Acoustic Sensor Pair. *Journal of Geophysical Rsearch: Solid Earth*, *123*, 6826–6844. https://doi.org/10.1029/2017JB015132

Nippress, A., Green, D. N., Marcillo, O. E., & Arrowsmith, S. J. (2014). Generating regional infrasound celerity-range models using ground-truth information and the implications for event location. *Geophysical Journal International*, *197*(2), 1154–1165. https://doi.org/10.1093/gji/ggu049

Park, J., Hayward, C., & Stump, B. W. (2018). Assessment of infrasound signals recorded on seismic stations and infrasound arrays in the western United States using ground truth sources. *Geophysical Journal International*, *213*(3), 1608–1628. https://doi.org/10.1093/gji/ggy042

Smith, C. M., & Gabrielson, T. B. (2020). Farfield coherent infrasound generation using an air-propane burner. *The Journal of the Acoustical Society of America*, *148*(5), 3181–3194. https://doi.org/10.1121/10.0002481

APPENDIX A. SUPPLEMENTAL MATERIAL

Here we include the detailed GCA-BAD method results for a variety of the stations discussed in the main report.

A.1. Tropospheric Arrivals from UTTR event on August 1, 2007

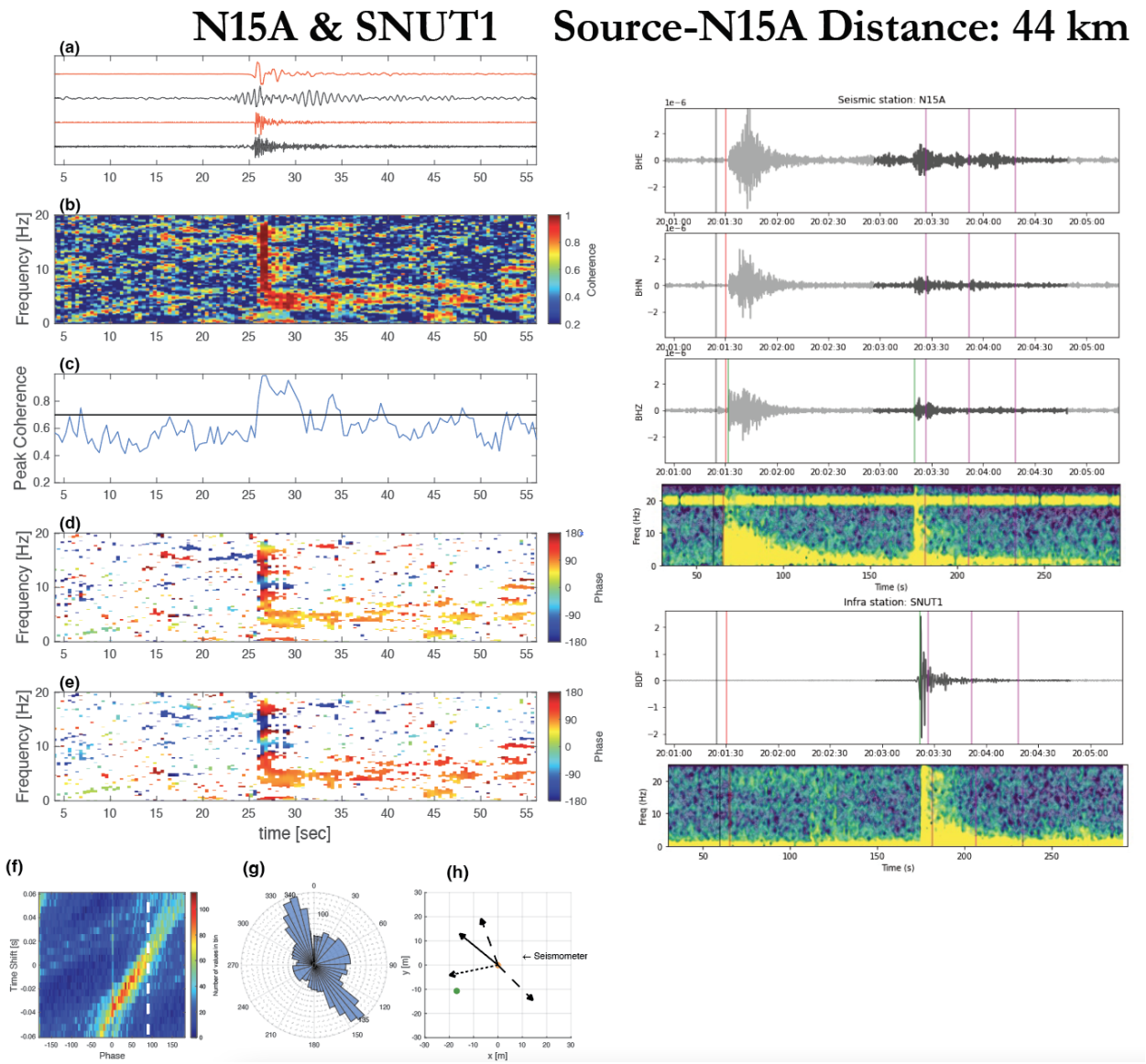

Figure A-1. GCA-BAD method results for signals from the UTTR August 1, 2007, event as recorded by seismic station N15A and infrasound station SNUT1.

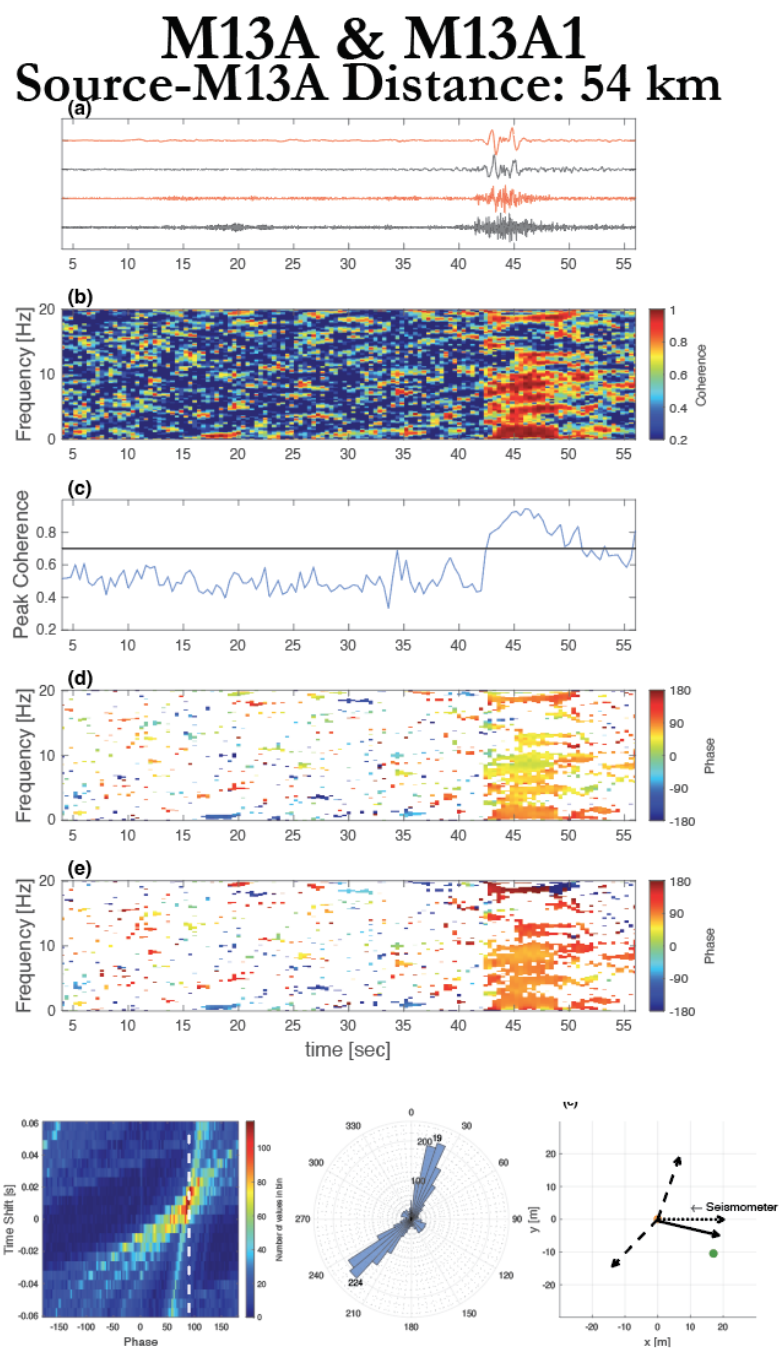

Figure A-2. GCA-BAD method results for signals from the UTTR August 1, 2007, event as recorded by seismic station M13A and infrasound station M13A1.

A.2. Stratospheric Arrival Bonus Results for November 21, 2020, Southern California Rocket Launch

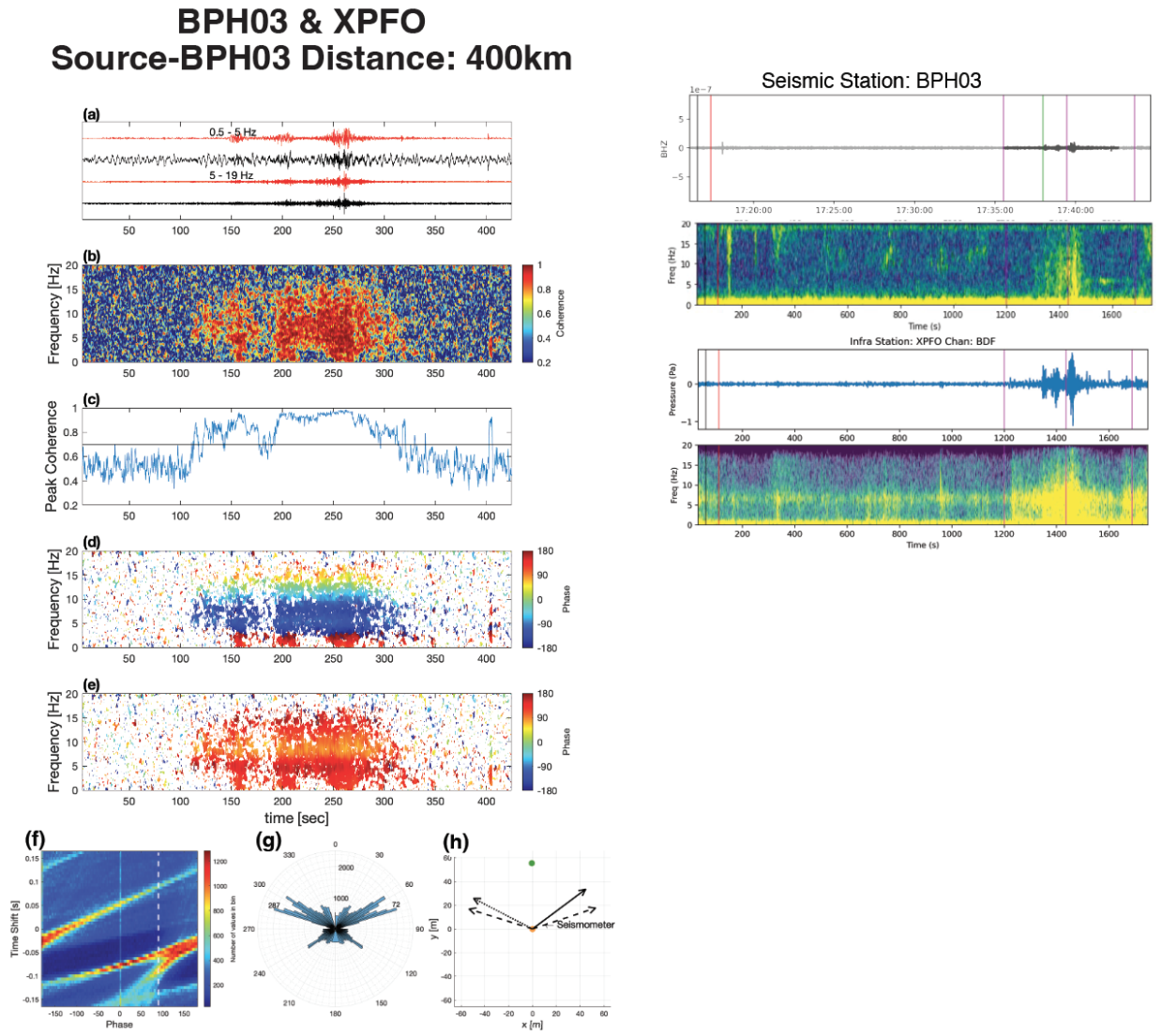

Figure A-3. GCA-BAD method results for signals from the November 21, 2020, rocket launch event as recorded by seismic station BPH03 and infrasound station XPF0.

A.3. Particle Motion from Seismic Stations HVU and BPH11

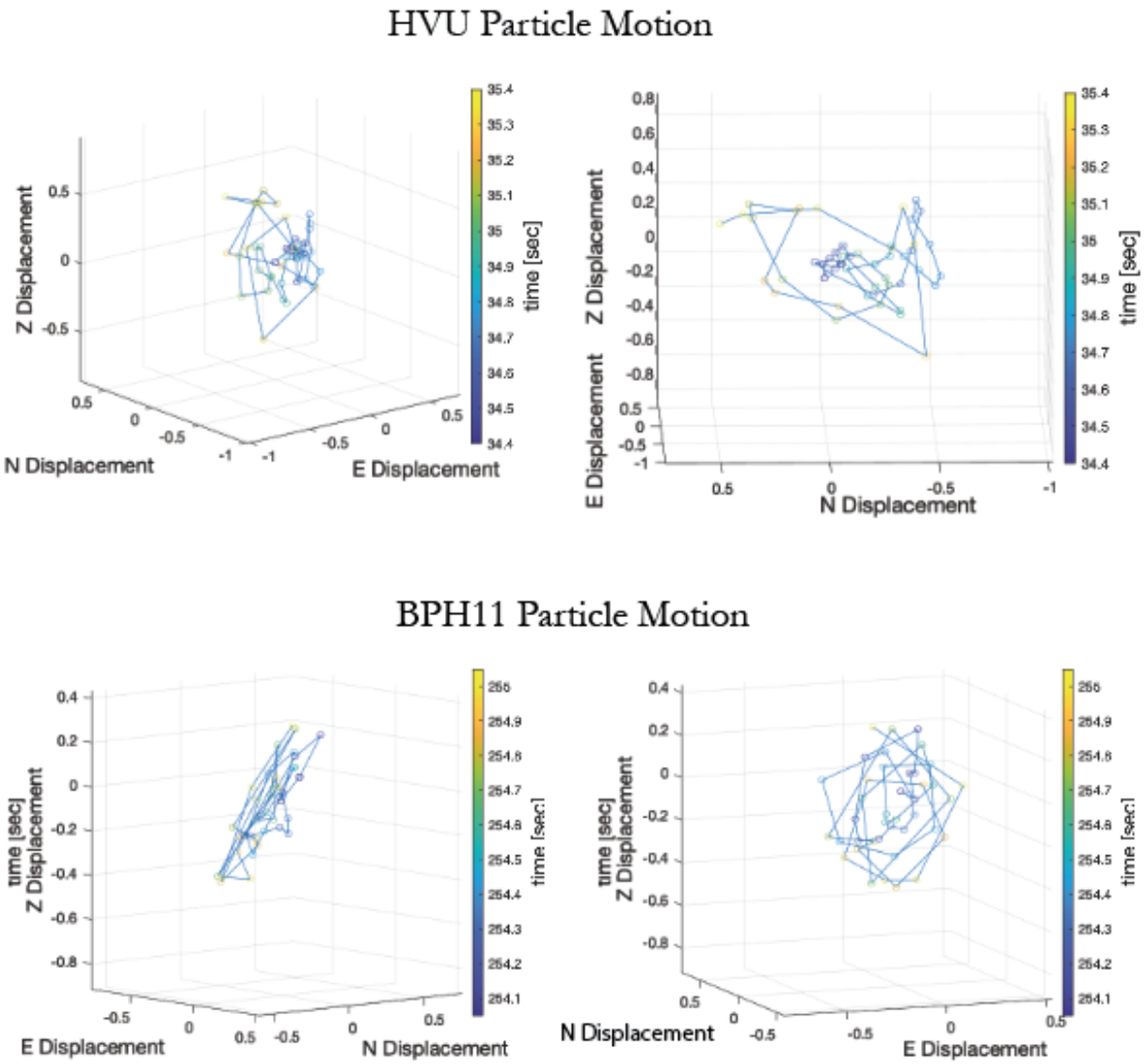

Figure A-4. Retrograde particle motion at different angles from seismic stations HVU (over coherent tropospheric arrivals) and BPH11 (over coherent stratospheric arrivals). The left and right have the same scales, so the left plots are minimizing the determined transverse component (less energy) while the right plots are approximately maximizing the radial components (more energy).

DISTRIBUTION

Email—Internal

Name	Org.	Sandia Email Address
Elizabeth Berg	6756	eliberg@sandia.gov
Clinton Koch	6756	clikoch@sandia.gov
Sarah Albert	6752	salber@sandia.gov
Fransiska Dannemann Dugick	6752	fkdanne@sandia.gov
Technical Library	1911	sanddocs@sandia.gov
Marlon Ramos	6756	mdramos@sandia.gov

Email—External

Name	Company Email Address	Company Name

Hardcopy—Internal

Number of Copies	Name	Org.	Mailstop

Hardcopy—External

Number of Copies	Name	Company Name and Company Mailing Address

This page left blank

Sandia National Laboratories

Sandia National Laboratories is a multimission laboratory managed and operated by National Technology & Engineering Solutions of Sandia LLC, a wholly owned subsidiary of Honeywell International Inc. for the U.S. Department of Energy's National Nuclear Security Administration under contract DE-NA0003525.